The Prominent Spring Bloom and Its Relation to Sea-ice Melt in the Sea of Okhotsk, Revealed by Profiling Floats

Sachiko Kishi[1], Kay I. Ohshima[2], Jun Nishioka[1], Noriaki Isshiki[3], Sohey Nihashi[4], and Stephen C. Riser[5]

[1]Hokkaido University
[2]Institute of Low Temperature Science, Hokkaido University
[3]Hiroo Town Hall
[4]National Institute of Technology, Tomakomai College
[5]University of Washington

November 23, 2022

Abstract

Seven profiling floats equipped with oxygen sensors deployed in the Sea of Okhotsk provide time series data for 33 cases of spring phytoplankton bloom, including nine cases in which sea ice existed just before the bloom (prior-ice case). As an index of biological productivity, we calculated Net Community Production (NCP) based on the increasing oxygen rate using the Redfield ratio. The total NCP in the euphotic layer averaged for prior-ice cases is 31.3 mmolCm^{-2}day^{-1}), ~4 times higher than that of non-ice cases. In addition to intensification of surface stratification, other factors of sea-ice melt likely enhance the bloom. The influence of sea-ice melt is particularly large in the southwestern region, where the iron availability likely limits phytoplankton growth. A suggested scenario is that when the sea ice containing sediment/iron is transported from the northern shelves, a prominent bloom is induced via the iron supply by sea-ice melt.

The Prominent Spring Bloom and Its Relation to Sea-ice Melt in the Sea of Okhotsk, Revealed by Profiling Floats

S. Kishi[1], K. I. Ohshima[2,3], J. Nishioka[2,3], N. Isshiki[1,4], S. Nihashi[5], and S. C. Riser[6]

[1]Graduate School of Environmental Science, Hokkaido University, Sapporo, Japan.

[2]Institute of Low Temperature Science, Hokkaido University, Sapporo, Japan.

[3]Arctic Research Center, Hokkaido University,Sapporo, Japan

[4]Hiroo Town Hall, Hiroo, Japan

[5]Department of Engineering for Innovation, National Institute of Technology, Tomakomai College, Tomakomai, Japan

[6]School of Oceanography, University of Washington, Seattle, WA, USA.

Corresponding author: S. Kishi(sachiko-k@ees.hokudai.ac.jp)

Key Points:

- Profiling floats equipped with oxygen sensors observed 33 cases of spring phytoplankton bloom in and around the Sea of Okhotsk, seasonal ice zone.
- Total Net Community Production estimated in the euphotic layer in cases where sea-ice existed is much higher than that of no ice cases.
- In addition to the intensification of surface stratification, sediment/iron released from melting sea-ice likely enhances the spring bloom.

Abstract

Seven profiling floats equipped with oxygen sensors deployed in the Sea of Okhotsk provide time series data for 33 cases of spring phytoplankton bloom, including nine cases in which sea ice existed just before the bloom (prior-ice case). As an index of biological productivity, we calculated Net Community Production (NCP) based on the increasing oxygen rate using the Redfield ratio. The total NCP in the euphotic layer averaged for prior-ice cases is 31.3 mmolCm^{-2}day^{-1}), ~4 times higher than that of non-ice cases. In addition to intensification of surface stratification, other factors of sea-ice melt likely enhance the bloom. The influence of sea-ice melt is particularly large in the southwestern region, where the iron availability likely limits phytoplankton growth. A suggested scenario is that when the sea ice containing sediment/iron is transported from the northern shelves, a prominent bloom is induced via the iron supply by sea-ice melt.

Plain Language Summary

The seasonal ice zone is a high biological productivity area with a large spring phytoplankton bloom. The enhanced biological production there results in significant CO_2 uptake, which could play an important role in global carbon budget. However, understanding of high biological productivity in seasonal ice zones is poor due to limited observations. This study examines the spring bloom in and around the Sea of Okhotsk, a typical seasonal ice zone, using profiling floats equipped with oxygen sensors. Based on the rate of oxygen increase for 33 cases of the spring bloom, we estimated NCP as a quantitative indicator of biological production and CO_2 uptake. It is statistically shown that a large spring bloom, corresponding to high NCP, is strongly related to sea-ice melt. The cause is suggested to be sediments/iron released from melting sea-ice as well as enhancement of stratification and light availability. This study will also provide the first attempt to evaluate the impact of significant sea-ice decline in the Sea of Okhotsk on the carbon budget in the present and future.

1 Introduction

The seasonal ice zone generally provides a rich marine ecosystem, mainly originating from large phytoplankton blooms associated with sea-ice melt. The Sea of Okhotsk, a marginal sea of the North Pacific, is a typical such ocean (Sorokin and Sorokin, 1999； Mustapha et al., 2009). For example, Kasai et al. (2010) reported that the chlorophyll-a concentration at a depth of 0–30m in this sea increases just after sea-ice melt and peaks in April as 1.8 ± 1.3 mg m^{-3}, which is much higher than that in the adjacent North Pacific (Shiozaki et al., 2014). Seasonal sea-ice likely plays an important role in the enhancement of this spring phytoplankton bloom (hereafter referred to as the spring bloom). Specifically, increased vertical stability of the freshwater supply associated with sea-ice melt enhances light availability. This provides a favorable condition for the increase in phytoplankton (Niebauer et al., 1990; Sorokin and Sorokin, 1999), in addition to the enhanced nutrient supply provided by convective mixing in the preceding winter.

Most of the subarctic Pacific is regarded as the High Nutrient Low Chlorophyll (HNLC) region, where the growth of phytoplankton is limited by iron (Tsuda et al., 2003). However, the Oyashio region of the western subarctic Pacific has relatively high biological productivity, likely due to the iron supply from the Sea of Okhotsk via intermediate water (Nishioka et al., 2007, 2013).

On the other hand, sea ice in southern region of the Sea of Okhotsk contains a higher concentration of iron than the underlying surface seawater, and the iron released by sea-ice melt provides a favorable condition for phytoplankton growth (Kanna et al., 2014; 2018). The enrichment of iron cannot be explained only by the atmospheric dust iron deposition onto the sea ice (Kanna et al., 2014). A part of sea ice in this region is transported from the shelf of Sakhalin Island and northwestern shelves of the Sea by the East Sakhalin Current and prevailing north wind (Simizu et al., 2014). Over these shelves, sedimentary materials including iron can be brought to the surface by the strong bottom currents and wintertime convection, and then incorporated into sea ice (Ito et al., 2017). Thus, there is a possibility that the iron in sea ice originates from the sedimentary materials over these shelves. However, all previous studies have been based on a snapshot observation or single-point moored measurement. Owing to logistical difficulties of measuring in sea ice in these areas, no continuous observations during the spring bloom have been made. Thus, our knowledge of the spring bloom in the Sea of Okhotsk is very limited.

A quantitative indicator of marine biological production associated with the spring bloom is the Net Community Production (NCP), which is equal to primary production minus respiration over all trophic levels. Estimations of NCP have been conventionally made by shipboard observations and/or moorings. However, these methods have a limitation in spatial coverage or monitoring period, and in general observations that focus on NCP have not been conducted in ice-covered regions. Riser and Johnson (2008) was the first study that estimated an NCP from profiling floats equipped with oxygen sensors. They estimated the NCP just below the mixed layer in the Pacific subtropical ocean, based on the time series data of the oxygen vertical profile, using the Redfield ratio. This work has been followed by additional studies, which estimated the seasonal or annual NCP in various regions (e.g., Sukigara et al., 2011, Bushinsky and Emerson, 2015, Yang et al., 2017). Some of these studies have validated the use of oxygen variation for estimation of NCP by comparing with estimates obtained from conventional methods. In recent years, Biogeochemical-Argo (BGC-Argo) floats, which can observe biogeochemical parameters such as oxygen, nitrate, pH, and chlorophyll-a, have been deployed globally (Claustre et al., 2020). Many BGC-Argo floats have been deployed in the Southern Ocean through the Southern Ocean Carbon and Climate Observations and Modeling (SOCCOM) project (Johnson et al., 2017; Riser et al., 2018). These floats have observed a large spring bloom associated with sea-ice melt in the Southern Ocean (Briggs et al., 2018).

In the Sea of Okhotsk, 30 profiling floats have been deployed since 1997 (Ohshima et al., 2014), and those which were deployed after 2007 were equipped with oxygen sensors and a sea-ice detection system. These floats can observe the time series of vertical profiles of water properties that cannot be captured by snapshot or satellite observations in this data-void region. Further, owing to the sea-ice detection system, the floats have provided year-round data including the ice-covered season. Thus it is expected that the dataset might reveal the detail of bloom development process inferred from the change in water properties and its relationship with sea-ice melt process.

In this study, we analyze the behavior of dissolved oxygen (DO) in the upper ocean during the spring bloom, based on time series data of the vertical profiles obtained from the profiling floats with oxygen sensors. The study focuses on the effect and mechanism of sea-ice melt on the spring bloom by estimating the NCP and comparing it with environmental conditions. The seven floats used in this study sampled a total of 33 cases of spring oxygen behavior over the course of 12 years, including 9 cases in which sea ice was present just before the spring bloom.

2 Data and Methods

2.1 Profiling float measurements

Seven profiling floats equipped with oxygen Optode sensors were deployed in the Sea of Okhotsk. The floats were ballasted to drift at a nominal depth of 1650 m and programmed to cycle on a 5- or 10-day schedule. Although the Optode oxygen sensors have some bias errors, approximately 0 to −40 μmol kg^{-1} for raw data and −3.1 ± 4.09 μmol kg^{-1} for calibrated data using the phase-domain method (Drucker and Riser., 2016), the sensor drift is negligible (Bushinsky et al., 2016) or only about 0.5% per year after deployment (preliminary analysis by Riser's laboratory). In this study, we used the variation of raw oxygen data during a relatively short period in order to estimate the NCP of spring bloom. Thus, the use of uncalibrated oxygen data is unlikely to affect the conclusions of this study, even though the absolute value could be somewhat biased.

Each float was equipped with a sea-ice detection system aimed at protecting the sensors from colliding with ice at the surface, as discussed in detail in Riser et al. (2018). When the float measures a temperature below a threshold value of −1.70 ºC in the near-surface mixed layer, close to the sea-ice formation temperature, it immediately descends to the parking depth. The float would continues to cycle without surfacing until the measurements exceed the threshold temperature. Since the float does not surface during the under-ice period, its position during these periods is unknown and is estimated by linear interpolation between its last and first known locations. The trajectories of the seven floats used in this study are shown in Figure 1. The observation period ranges from November 2007 to December 2019 and covers 33 cases of spring blooms.

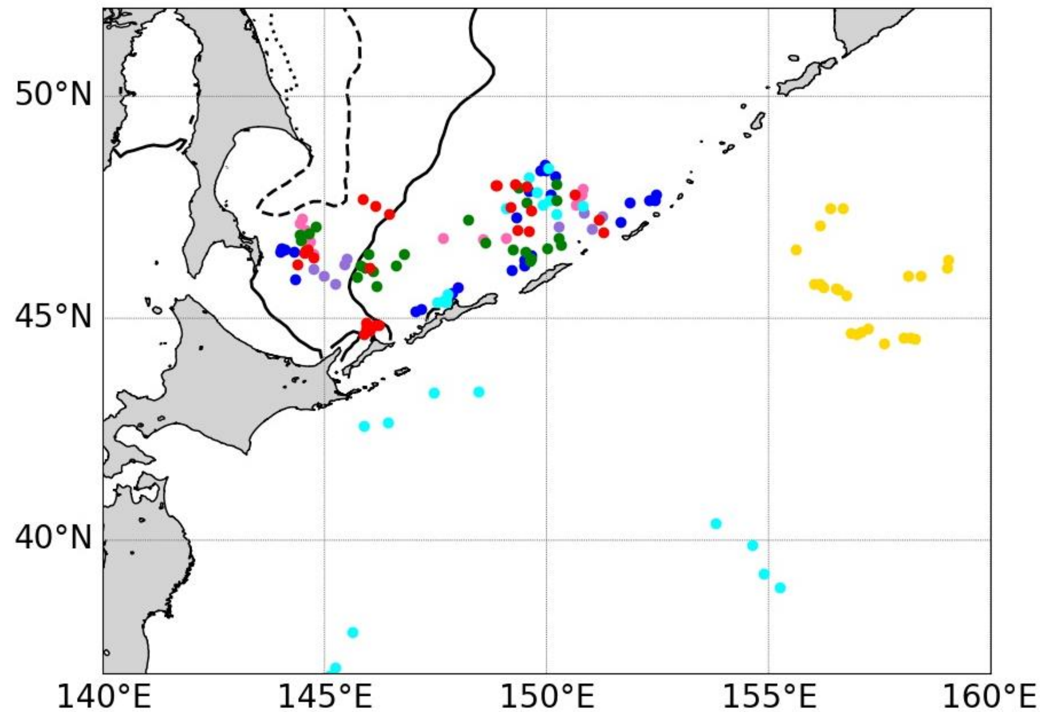

Figure 1. Trajectories of seven profiling floats from November 2007 to December 2019. Colored circles indicate the float locations in April or May (spring bloom period). The black contours in the Sea of Okhotsk shows the sea-ice edge (defined as 15% ice concentration) averaged over 2007-2018 for March (solid), April (dashed), and May (dotted).

2.2 Sea ice and wind data

The presence of sea ice was determined by the daily ice concentration estimate from the Advanced Microwave Scanning Radiometers (AMSR-E/2) and the Special Sensor Microwave/Imager (SSM/I), as well as by the temperature threshold of the floats. The ice concentration was estimated by using the Bootstrap algorithm (Comiso, 1995). When the ice concentration averaged within a radius of 100 km around a float's surfacing position was above 30%, the area was defined as having sea ice (the gray shaded region in Figure 2). Among the 33 cases of the spring bloom, nine cases had sea ice just prior to the spring bloom.

The surface DO concentration is affected by various biological and physical factors. Air-sea gas exchange is the main physical factor and is a function of wind speed and temperature. To infer the magnitude of air-sea gas exchanges, we used daily wind speed at 10-m height from the

European Centre for Medium-Range Weather Forecasts Re-Analysis (ERA5) dataset, at grid points located closest to the surfacing locations of the floats.

2.3 Calculation of NCP

Because oxygen concentration also depends on seawater temperature and salinity, its variation is not necessarily simple . In this study, we used the oxygen anomaly ΔO_2 (oxygen concentration minus oxygen solubility), corresponding to negative AOU (Apparent Oxygen Utilization), to minimize the dependency on temperature and salinity. We followed the method by Riser and Johnson (2008) and calculated the NCP by using the rate of oxygen increase in spring. The period of the spring bloom is defined as the end of March through mid-May (40–50 days), and the rate of oxygen production is determined from the slope of straight lines fitted by least squares to the ΔO_2 data during each spring season. NCP rates are then estimated from these slopes at depths in the euphotic layer by converting oxygen production to carbon uptake using the Redfield ratio (150 moles of O_2 produced per 106 moles of CO_2 fixed; (Anderson, 1995).

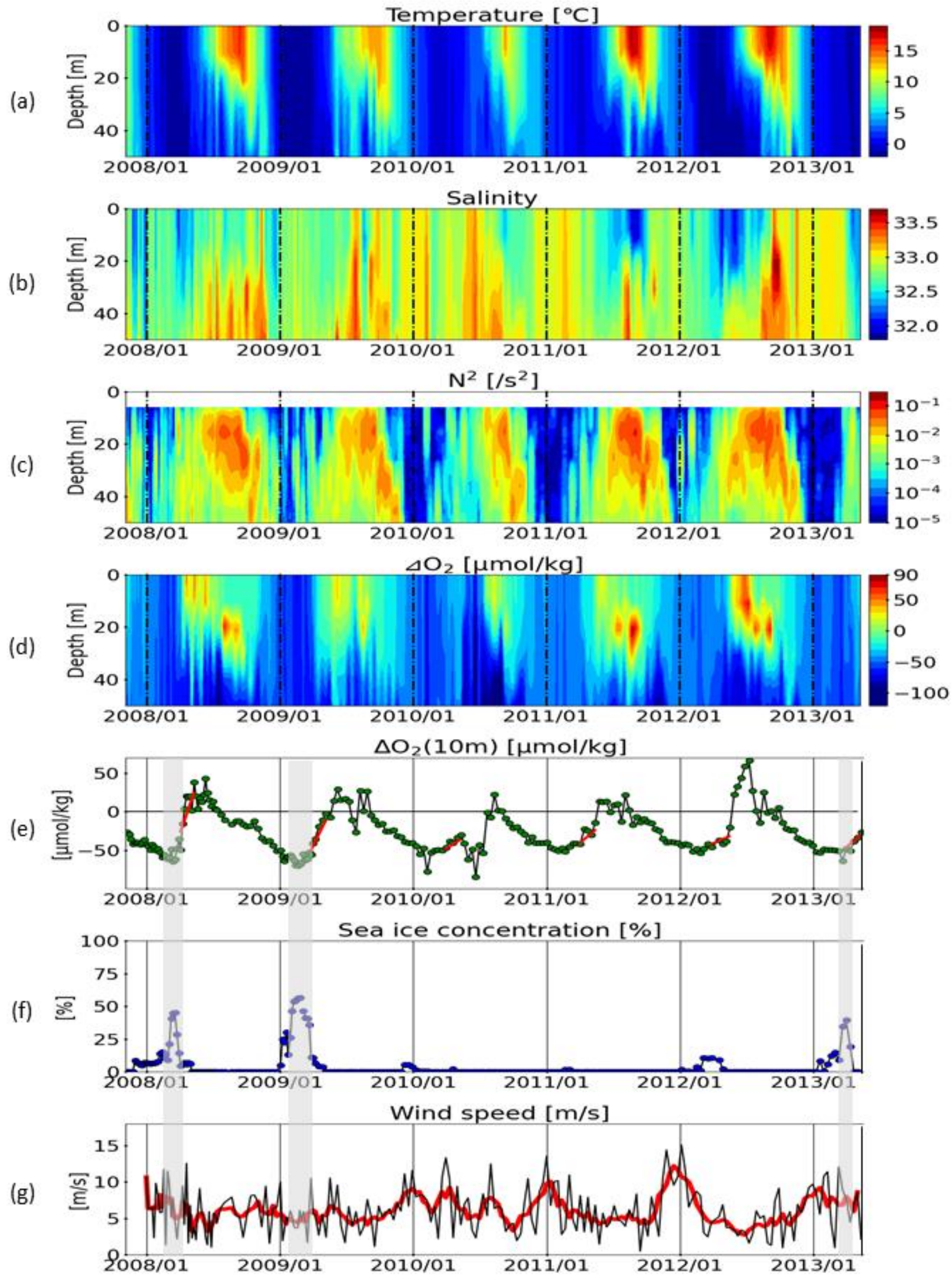

Figure 2. Time series of vertical profiles of (a) temperature, (b) salinity, (c) buoyancy frequency squared, represent as N^2 (d) ΔO_2 and (e) ΔO_2 at 10 m for float 5259 (red in Figure 1), and (f) sea-ice concentration from SSM/I and (g) wind speed from ECMWF, from October

2007to May 2013. The red lines in (e) indicate least-squares fits, showing the increase rate of ΔO_2 during the spring bloom. The gray shades in (e)~(g) highlight the periods of sea-ice melt.

3 Results and Discussion

3.1 Time series of float data

Time series of temperature, salinity, buoyancy frequency, and ΔO_2 from one of the profiling floats are shown in Figure 2, together with the sea-ice concentration and wind speed at the float locations. The float data clearly capture the seasonal cycle of the upper ocean. It is found that ΔO_2 at the depth of 10 m (Figure 2e) increased during spring (from the end of March to mid-May) in each year. However, the increasing rate of ΔO_2, estimated via least-squares fitting (the red line in Figure 2e), seems to depend on the observation year or position. The increasing rate is significantly higher in cases when sea-ice cover existed just before the estimate (referred to as the prior-ice case), specifically in 2008 and 2009, than in cases with no prior sea-ice cover (referred to as non-ice case), specifically in 2010, 2011, and 2012. Such characteristics are commonly observed by the other six floats (see supplementary Figures S2 to S6). In addition to the spring bloom, ΔO_2 shows a delayed peak at the surface from June to July in 2012, and a subsurface peak (20–30 m) from July to August in 2008, 2011, and 2012. This subsurface peak is consistent with the enhanced biological production characterized as a subsurface chlorophyll-a maximum in summer, as reported by Kasai et al. (2010). The analysis in this study focuses only on the spring bloom, which occurs from the end of March to mid-May, for examining the relationship between sea-ice melt and the spring bloom.

Wind speeds in the observational area were generally higher in winter and lower in spring (Figure 2g). Variations of surface ΔO_2 (Figure 2d) do not show those expected from the wind variation, e.g. oxygen supersaturation over 100–110 % occurred in April and May, even though the wind speed weakened in these months. As this tendency also occurred for the other floats (see supplementary Figures S2 to S6), the data suggest that these periods of supersaturation are not governed by air-sea gas exchanges that are controlled by wind speed. Furthermore, although the near-surface stratification in each spring was relatively strong, the increase in ΔO_2 at depth to 50 m occurred simultaneously. These suggest that this increment was caused mainly by in situ photosynthesis-related proceses rather than by the atmospheric O_2 uptake.

After sea-ice melt, a salinity deficit occurs at the ocean surface. Two examples of a vertical profile of salinity just after the ice melt and that of oxygen increment during the spring bloom are shown in Figure 3a-b. The two profiles correspond well to each other. From the decrease of salinity, the content ratio of meltwater can be estimated based on the mixing ratio of salinity in sea ice (4.6 psu in the Sea of Okhotsk) and salinity in the source water (at the depth just below the base of the low salinity layer). We have estimated the meltwater ratio from all the prior-ice cases at 5 m intervals, and examined its relationship with the oxygen increment (Figure 3c). A relatively strong correlation between the two (Correlation coefficient R is 0.65) supports the idea that the oxygen increment due to photosynthesis is induced by the meltwater input, and further suggests that the strength of the spring bloom is governed by the amount of meltwater.

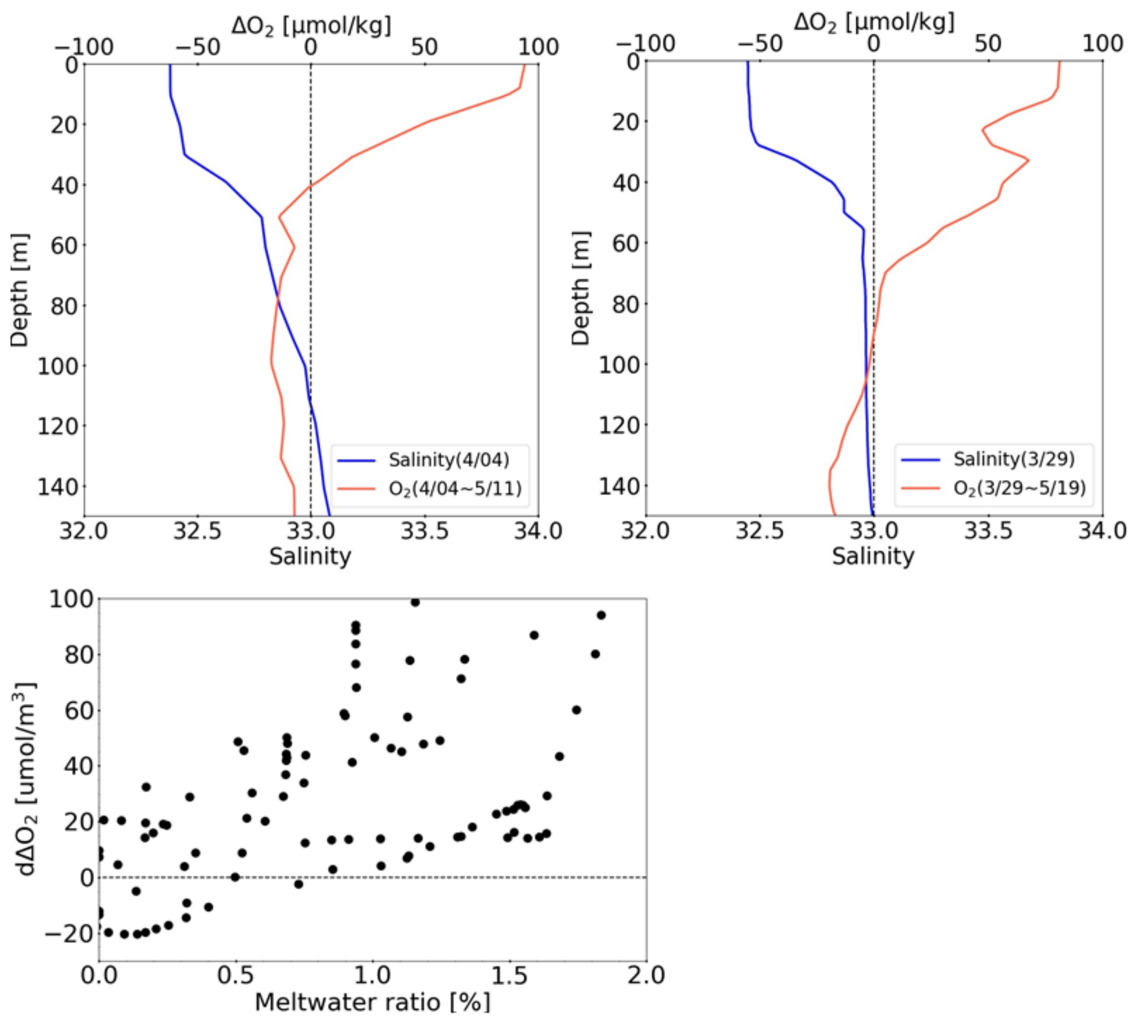

Figure 3. Vertical profiles of salinity just after sea-ice melt (blue lines) and of DO increment during the spring bloom (red lines) for (a) the 2008 bloom (44.8°N, 146.0°E) and (b) the 2018

bloom (46.5°N, 144.1°E). (c) Plots of meltwater ratio versus oxygen increment during the spring bloom, estimated from all the prior-ice cases at 5 m intervals.

3.2 Estimation of NCP

The averaged vertical profiles of NCP derived from the float observations during the spring bloom are shown in Figure 4a, for prior-ice cases (9 cases) and non-ice cases (16 cases) in the Sea of Okhotsk, and for cases in which the floats were located in the North Pacific (8 cases). The NCP is by far highest in prior-ice cases, and the difference is more prominent near the surface. The total NCP for each individual spring bloom was calculated by vertical integration of the NCP profile data from 50 m to the surface, assumed to be the euphotic layer (Figure 4b). Calculations from greater depths show similar results: Calculations from 70 m result in the NCP increase only by less than 10% on average. The total NCP averaged for prior-ice cases is 31.1 [mmolCm^{-2}day^{-1}], which is 4.1 times higher than the 7.6 mmolCm^{-2}day^{-1} of non-ice cases (99% significance by the Student t-test). This value is comparable to that in the Southern Ocean, known as the high biological production area (Thomalla et al., 2015). On average, the total biological production during the spring bloom period is 1374 mmolC m^{-2} for prior-ice cases and 576 mmol C m^{-2} for non-ice cases. Note that air-sea gas exchanges are not considered in these NCP estimates. Since gas exchange would occur from sea to air when DO in the sea is supersaturated, the NCP found in this study probably tends to be an underestimate. However, as described in section 3.1, it is likely that the oxygen increment in spring is mainly due to photosynthesis by biological production, and a qualitative discussion of the relationship between NCP and sea-ice melt is still adequate.

3.3 Effects of sea-ice melt

A spring bloom is a rapid biological increment occurring in mid- to high latitudes due to the increase in sea temperature and solar illumination, which improve the environment for biological production. The current work is the first observation-based study that reveals the onset of a spring bloom induced by sea-ice melt in the Sea of Okhotsk, by showing significantly higher NCP in the prior-ice cases than in the non-ice cases. The analysis will now focus on how sea-ice melt affects the occurrence of spring bloom. This issue has not previously been well-understood ,although the intensification of stratification at the surface layer from warming and the freshwater supply has been regarded as an important factor (Sullivan et al., 1993). Here, we compare the NCP values with the buoyancy frequency squared (N^2) averaged over 25–35 m depths (Figure 4c). In spring, the surface layer stratification is intensified regardless of the presence of melting sea-ice. When no sea ice is present, the increase in stratification is caused solely by surface warming. When sea ice was present just before, the near-surface stratification is increased by freshwater input by ice melting as well. On average, N^2 is 2.95×10^{-3} ($/s^2$) for prior-ice cases, somewhat higher than the value of 2.07×10^{-3} ($/s^2$) for non-ice cases. However, no significant correlation exists between the stratification and NCP (R= 0.21) when considering the whole data set. For similar N^2 levels, the NCP tends to be higher in prior-ice cases than in non-ice cases (Figure 4c). These results suggest that the change in stratification is not the only reason why sea-ice melt leads to a massive spring bloom.

The locations of each spring bloom are plotted as circles in Figure 4d, with their size being proportional to the NCP values. Among the nine blooms in the western part of the Kuril Basin, defined as west of 147°E, the NCP value is significantly larger in the prior-ice cases (red) than in the non-ice cases (blue), by a factor of 7.5 on average. In contrast, among 15 blooms in the eastern part of the Kuril Basin, defined as east of 147°E, there is no significant difference in the NCP value in cases between the prior-ice and non-ice cases. In the Sea of Okhotsk, the sea ice formed in the Sakhalin and northwestern shelves may incorporate bottom sediments containing iron, via strong winter convection reaching the bottom (Ito et al., 2017); after formation, the ice drifts to the southwestern region of the Sea of Okhotsk. We assume that a part of sea ice found in the southwestern part of the Sea originates from these shelves, whereas sea ice in the eastern Sea is locally formed in the Kuril Basin. We propose that the difference in the origin of sea ice explains the varying influence of sea-ice melt on the NCP.

It is also noted that, when comparison is made for all the non-ice cases in the Sea of Okhotsk, the NCP tends to be larger in the area closer to the Kuril Straits. It is possible that this is results from advection of water including high nutrients and iron via the strong tidal mixing around the Kuril Straits (Nishioka et al., 2013).

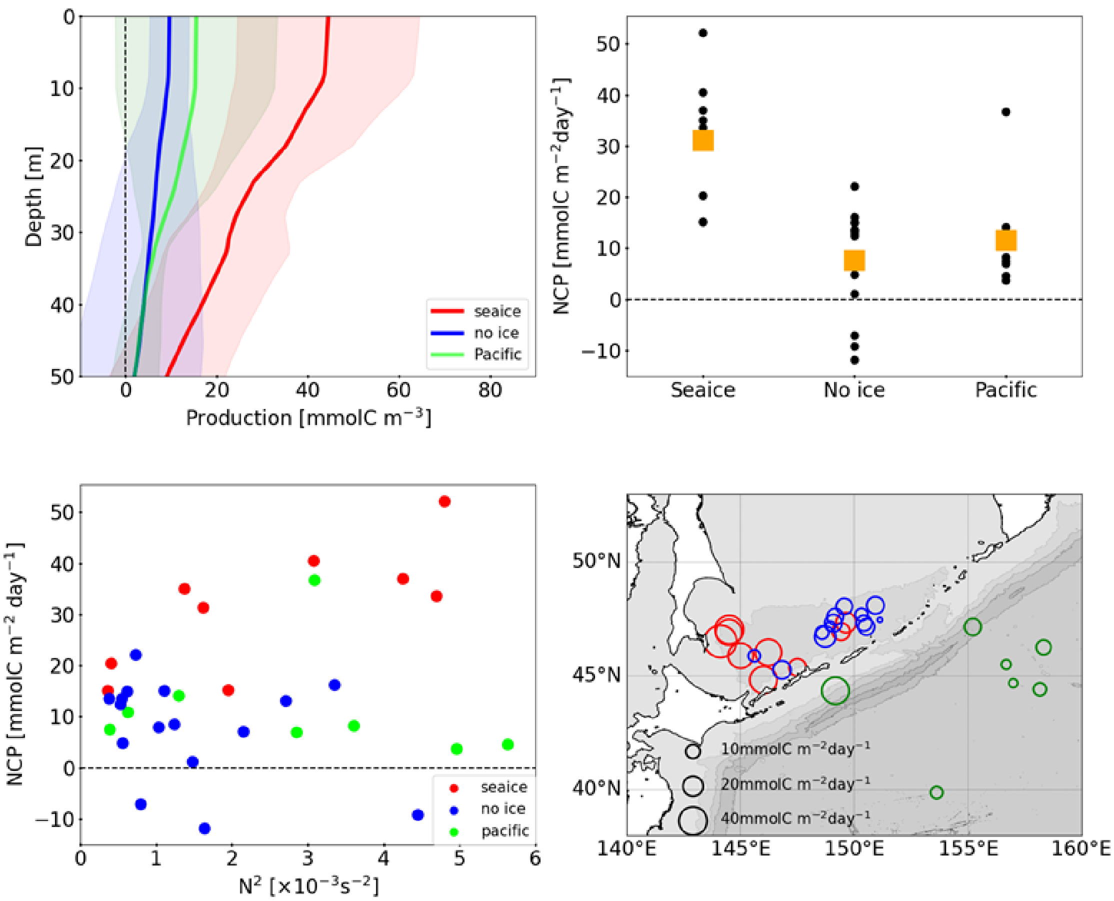

Figure 4. (a) Vertical profiles of NCP averaged for (red) prior-ice cases and (blue) non-ice cases in the Sea of Okhotsk and (green) cases in the North Pacific, with the standard deviations (indicated by shadings). (b) Total NCP integrated over the blooming layer for individual spring bloom (black dots) and the average (orange dots) classified into prior-ice cases and non-ice cases in the Sea of Okhotsk and cases in the North Pacific. (c) Plots of buoyancy frequency squared at a depth of 30 m versus total NCP. (d) Spatial distributions of total NCP during spring bloom, with the circle size being proportion to the NCP value. The color coding in (c) and (d) follows that of (a). The contours in (d) indicate 50 m depth, obtained by the General Bathymetric Chart of the Oceans.

4 Concluding remarks

Seven profiling floats equipped with oxygen sensors have provided time series data for 33 cases of spring blooms, including nine cases in which sea ice existed just before the spring bloom began (the prior-ice case), in and around the Sea of Okhotsk. Accumulation of these data makes it possible to evaluate statistically the effects of sea-ice melt on the spring bloom. All cases show that the oxygen in the surface layer increased during the spring, defined as the end of March to mid-May. As an index of biological productivity during the spring bloom, we estimated NCP based on the rate of oxygen increase and the Redfield ratio for all 33 cases. The average total NCP in the euphotic layer is 31.3 (mmol C $m^{-2}day^{-1}$) in the prior-ice case is ~4 times higher than that in the non-ice case. This demonstrates that the sea-ice melt is a key factor for the prominent spring bloom.

We have examined how sea-ice melt affects the spring bloom. We used the buoyancy frequency squared averaged over depths of 25–35 m (typical euphotic zone depths) as an index of the stratification intensity during the spring bloom, and investigated its relationship with the total NCP. The NCP is always higher in the prior-ice cases than in the non-ice cases for similar buoyancy frequencies (Figure 4c). This suggests that other factors by sea-ice melt substantially enhance the spring bloom, in addition to the intensification of surface stratification.

In the Southern Ocean, a large spring bloom is likely to occur in many sea-ice melt regions (e.g., Briggs et al., 2018). In the case of the Sea of Okhotsk, the influence of sea-ice melt on the spring bloom seems to depend on the region. The influence of sea-ice melt is clearly identified in the southwestern region of the Sea of Okhotsk, while such influence is not so clear in the eastern region of the Kuril Basin. In the southwestern region of the Kuril Basin, where iron availability likely limits phytoplankton growth, only when the sea ice containing the sediment/iron is transported from the northern shelves, a prominent spring bloom is induced via the ice-supplied iron. While in the eastern region, water advected from the Kuril Straits may have supplied some iron from the lower layer via strong tidal mixing (Nishioka et al., 2013).

In this study, we estimated the NCP during the spring bloom in and around the Sea of Okhotsk, using the oxygen variability observed by a suite of profiling floats. Although our estimate is useful for evaluating the effect of sea-ice melt, the NCP estimates have some error, mainly because the component of air-sea gas (oxygen) exchange cannot be incorporated. More accurate estimation would require time series data of nutrients such as nitrate and/or chlorophyll-a. The deployment of BGC profiling floats, which would make such observation possible, will be needed in the future. One ultimate goal, initiated from this study, is to examine the CO_2 budget associated with the biological productivity in the Sea of Okhotsk and to determine the net exchange of CO_2 between the Sea and the atmosphere throughout the annual cycle. For such a purpose, the annual NCP must be estimated with evaluation of biological productivity in other seasons, such as during the subsurface summer phytoplankton bloom in addition to the spring bloom.

Acknowledgments

Deployments of profiling floats were made under the cooperative study by Hokkaido University and the University of Washington, The profiling floats were prepared at the University of Washington by Dana Swift, Rick Rupan, and Dale Ripley through NOAA grant NA15OAR4320063 to the Joint Institute for the Study of the Atmosphere and Ocean. We thank Naoya Kanna, Masato Ito and Vigan Mensah for discussion on this study. This work was supported by Grants-in-Aids for Scientific Research (17H01157 and 20H05707) from the Ministry of Education, Culture, Sports, Science and Technology in Japan.

Data Availability Statement

The AMSR-E and SSM/I data were obtained from website of the National Snow and Ice Data Center, University of Colorado (https://nsidc.org/data/ae_si12/versions/3; https://nsidc.org/data/ae_si6/versions/3). The AMSR2 data were provided by the Japan Aerospace Exploration Agency website (https://gportal.jaxa.jp/gpr/). The ERA5 reanalysis data were obtained from the ECMWF Research Data Server (https://cds.climate.copernicus.eu/cdsapp#!/dataset/reanalysis-era5-single-levels?tab=overview). The data set of profiling floats can be seen from the website (http://runt.ocean.washington.edu/hu/)

References

Anderson, L. A. (1995). On the hydrogen and oxygen content of marine phytoplankton, *Deep Sea Research, Part I, 42,* 1675–1680. https://doi.org/10.1016/0967-0637(95)00072-E

Briggs, E. M., Martz, T. R., Talley, L. D., Mazloff, M. R., Johnson, K. S. (2018). Physical and biological drivers of biogeochemical tracers within the seasonal sea ice zone of the

Southern Ocean from profiling floats. *Journal of Geophysical Research: Oceans, 123, 2,* 746–758. https://doi.org/10.1002/2017JC012846

Bushinsky, S. M., and Emerson, S. (2015). Marine biological production from in situ oxygen measurements on a profiling float in the subarctic Pacific Ocean. *Global Biogeochemical Cycles, 29,* 2050–2060. https://doi.org/10.1002/2015GB005251

Bushinsky, S.M., Emerson, S.R., Riser, S.C., Swift, D.D. (2016). Accurate oxygen measurements on modified Argo floats using in situ air calibrations. *Limnology and Oceanography: Methods, 14*, 491–505. http://dx.doi.org/10.1002/lom3.10107.

Claustre, H., Johnson, K. S. and Takeshita, Y. (2020). Observing the global ocean with Biogeochemical-Argo. *Annual Review of Marine Science, 2020,* 12:23–48. https://doi.org/10.1146/annurev-marine-010419-010956

Comiso, J. C. (1995). SSM/I Sea Ice Concentrations Using the Bootstrap Algorithm. *National Aeronautics and Space Administration Reference publication, 1380,* 49

Drucker, R. and Riser, S. C. (2016). In situ phase-domain calibration of oxygen Optodes on profiling floats. *Methods in Oceanography, 17,* 296–318. https://doi.org/10.1016/j.mio.2016.09.007

Ito, M., Ohshima, K. I., Fukamachi, Y., Mizuta, G., Kusumoto, Y. and Nishioka, J. (2017). Observations of frazil ice formation and upward sediment transport in the Sea of Okhotsk: A possible mechanism of iron supply to sea ice. *Journal of Geophysical Research: Oceans 122,* 788–802. https://doi.org/10.1002/2016JC012198

Johnson, K. S., Plant, J. N., Coletti, L. J., Jannasch, H. W., Sakamoto, C. M., Riser, S. C., Swift, D. D., Williams, N. L., Boss, E., Haentjens, N., Talley, L. D. and Sarmiento, J. L. (2017). Biogeochemical sensor performance in the SOCCOM profiling float array, *Journal of Geophysical Research: Oceans, 122,* 6416–6436. https://doi.org/10.1002/2017JC012838

Kanna, N., Toyota, T. and Nishioka, J. (2014) Iron and macro-nutrient concentrations in sea ice and their impact on the nutritional status of surface waters in the southern Okhotsk Sea, *Progress in Oceanography, 126,* 44–57. https://doi.org/10.1016/j.pocean.2014.04.012

Kanna, N., Sibano, Y., Toyota, T. and Nishioka, J. (2018). Winter iron supply processes fueling spring phytoplankton growth in a sub-polar marginal sea, the Sea of Okhotsk: Importance of sea ice and the East Sakhalin Current. *Marine Chemistry, 206,* 109–120. https://doi.org/10.1016/j.marchem.2018.08.006

Kasai, H., Nakano, Y., Ono, T. and Tsuda, A. (2010). Seasonal change of oceanographic conditions and chlorophyll a vertical distribution in the southwestern Okhotsk sea during the non-iced season, *Journal of Oceanography, 66,* 13–26. https://doi.org/10.1007/s10872-010-0002-3

Mustapha, M. A., Sei-Ichi, S. and Lihan T. (2009). Satellite-measured seasonal variations in primary production in the scallop-farming region of Okhotsk Sea. *ICES Journal of Marine Science, 66, 7,* 1557–1569. https://doi.org/10.1093/icesjms/fsp142

Niebauer, H. J., Alexander, V. and Henrichs, S. (1990). Physical and biological oceanographic interaction in the spring bloom at the Bering Sea marginal ice edge zone. *Journal of Geophysical Research: Oceans, 95,* C12. https://doi.org/10.1029/JC095iC12p22229

Nishioka, J., Ono, T., Saito, H., Nakatsuka, T., Takeda, S., Yoshimura, T., Suzuki, K., Kuma, K., Nakabayashi, S., Tsumune, D., Mitsudera, H., Johnson, W. K. and Tsuda, A. (2007). Iron supply to the western subarctic Pacific: Importance of iron export from the Sea of Okhotsk. *Journal of Geophysical Research: Oceans, 112,* C10. https://doi.org/10.1029/2006JC004055

Nishioka, J., Nakatsuka, T., Watanabe, Y. W., Yasuda, I., Kuma, K., Ogawa, H., Ebuchi, N., Scherbinin, A., Volkov, Y. N., Shiraiwa T. and Wakatsuchi, M. (2013) Intensive mixing along an island chain controls oceanic biogeochemical cycles. *Global Biogeochemical Cycles, 27,* 920–929. doi:10.1002/gbc.20088

Ohshima, K. I., Nakanowatari, T., Riser, S., Volkov, Y. and Wakatsuchi, M. (2014). Freshening and dense shelf water reduction in the Okhotsk Sea linked with sea ice decline. *Progress in Oceanography, 126,* 71–79. https://doi.org/10.1016/j.pocean.2014.04.020

Riser, S. C. and Johnson, K. S. (2008). Net production of oxygen in the subtropical ocean, *Nature, 451,* 327–325. https://doi.org/10.1038/nature06441

Riser, S. C., D. Swift, and R. Drucker (2018). Profiling floats in SOCCOM: technical capabilities for studying the Southern Ocean. *Journal of Geophysical Research: Oceans, 123,* 4055–4073, https://doi.org/10.1002/2017JC013419

Shiozaki, T., Ito, S., Takahashi, K., Saito, H., Nagata, T., Furuya, K. (2014). Regional variability of factors controlling the onset timing and magnitude of spring algal blooms in the northwestern North Pacific. *Journal of Geophysical Research: Oceans, 119,* 253–265. https://doi.org/10.1002/2013JC009187

Simizu, D., Ohshima, K. I., Ono, J., Fukamachi, Y. and Mizuta, G. (2014). What drives the southward drift of sea ice in the Sea of Okhotsk? *Progress in Oceanography, 126,* 33–43. https://doi.org/10.1016/j.pocean.2014.05.013

Sorokin, Y. I. and Sorokin, P. Y. (1999). Production in the Sea of Okhotsk. *Journal of Plankton Research, 21, 2,* 201–230. https://doi.org/10.1093/plankt/21.2.201

Sukigara, C., Suga, T., Saino, T., Toyama, K., Yanagimoto, D., Hanawa, K. and Shikama, N. (2011). Biogeochemical evidence of large diapycnal diffusivity associated with the subtropical mode water of the North Pacific, *Journal of Oceanography, 67,* 77–85. https://doi.org/10.1007/s10872-011-0008-5

Sullivan, C. W., Arrigo, K. R., McClain, C. R., Comiso, C. and Firestone, J. (1993). Distributions of phytoplankton blooms in the Southern Ocean. *Science, 262,* 1832–1837. https://doi.org/10.1126/science.262.5141.1832

Thomalla, S. J., Racault, M. F., Swart, S. and Monteiro P. M. S. (2015). High-resolution view of the spring bloom initiation and net community production in the Subantarctic Southern Ocean using glider data, *ICES Journal of Marine Science, 72,* 1999–2020. https://doi.org/10.1093/icesjms/fsv105

Tsuda, A., Takeda, S., Saito, H., Nishioka, J., Nojiri, Y., Kudo, I., Kiyosawa, H., Shiomoto, A., Imai, K., Ono, T., Shimamoto, A., Tsumune, D., Yoshimura, T., Aono, T., Hinuma, A., Kinugasa, M., Suzuki, K., Sohrin, Y., Noiri, Y., Tani, H., Deguchi, Y., Tsurushima, N., Ogawa, H., Fukami, K., Kuma, K., Saino, T. (2003). A mesoscale iron enrichment in the western subarctic Pacific induces a large centric diatom bloom. *Science, 300,* 958–961. https://doi.org/10.1126/science.1082000

Yang, B., Emerson, S. R. and Bushinsky, S. M. (2017). Annual net community production in the subtropical Pacific Ocean from in situ oxygen measurements on profiling floats, *Global Biogeochemical Cycles, 31,* 728–744. https://doi.org/10.1002/2016GB005545

AGU PUBLICATIONS

Geophysical Research Letters

Supporting Information for

The Prominent Spring Bloom and Its Relation to Sea-ice Melt in the Sea of Okhotsk, Revealed by Profiling Floats

S. Kishi[1], K. I. Ohshima[2,3], J. Nishioka[2,3], N. Isshiki[1,4], S. Nihashi[5], and S. C. Riser[6]

[1]Graduate School of Environmental Science, Hokkaido University, Sapporo, Japan.

[2]Institute of Low Temperature Science, Hokkaido University, Sapporo, Japan.

[3]Arctic Research Center, Hokkaido University, Sapporo, Japan.

[4]Hiroo Town Hall, Hiroo, Japan

[5]Department of Engineering for Innovation, National Institute of Technology, Tomakomai College, Tomakomai, Japan.

[6]School of Oceanography, University of Washington, Seattle, WA, USA.

Contents of this file

Introduction

This supporting information includes status of the profiling floats (Table S1) and the time series for six of the seven profiling floats (float 5259 is shown in Figure 2 in the manuscript (Figures S1 to S6)).

Table S1.

Float ID, First and Last profile date, Number of Profiles, First profile in the North Pacific, and Initial Location

Float ID	First Profile	Last Profile	Number of Profiles	First Profile in the North Pacific	Initial Location
5259	04 Nov 2007	11 May 2013	229	-	44.90N 145.19E
5260	05 Nov 2007	31 Oct 2012	210	-	45.40N 145.13E
6404	18 Nov 2010	21 Nov 2016	208	23 Feb 2014	44.83N 145.45E
9001	02 Jun 2013	04 Dec 2018	183	18 Feb 2014	45.34N 145.33E
9021	02 Jun 2013	04 Dec 2019	219	-	45.17N 144.94E
9049	09 Jun 2014	02 Feb 2017	96	-	45.16N 144.92E
9050	09 Jun 2014	13 Sep 2017	116	-	45.37N 145.12E

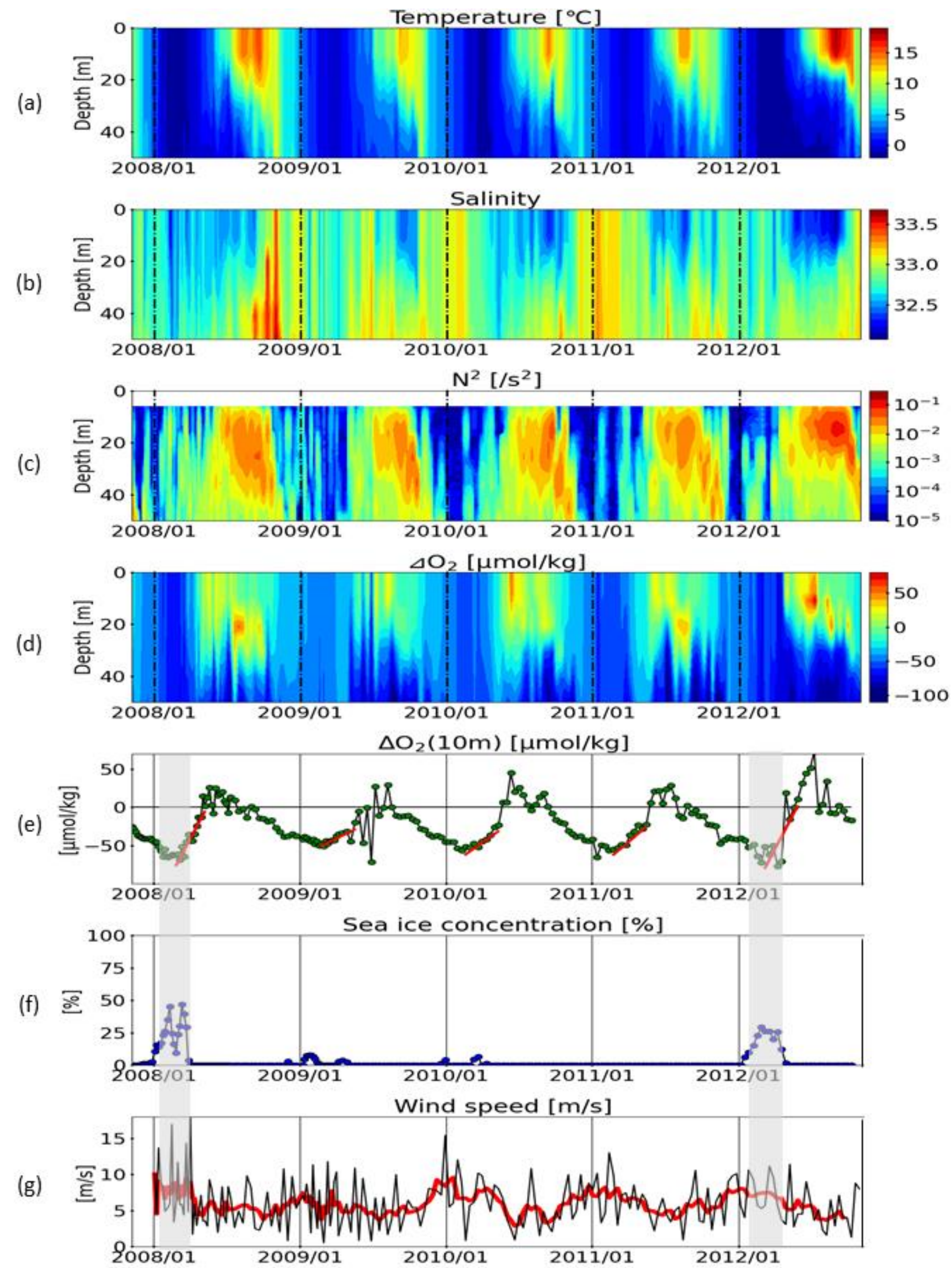

Figure S1

Time series of vertical profiles of (a) temperature, (b) salinity, (c) buoyancy frequency squared, represent as N^2, (d) ΔO_2 and (e) ΔO_2 at 10m for float 5260 (green in Fig.1) and (f) sea-ice concentration from SSM/I and (g) wind speed from ECMWF. The red lines in (e) indicate least-squares fitting, showing the increase rate of ΔO_2 during the spring bloom. The gray shades in (e)~(g) highlight the periods of sea-ice melt.

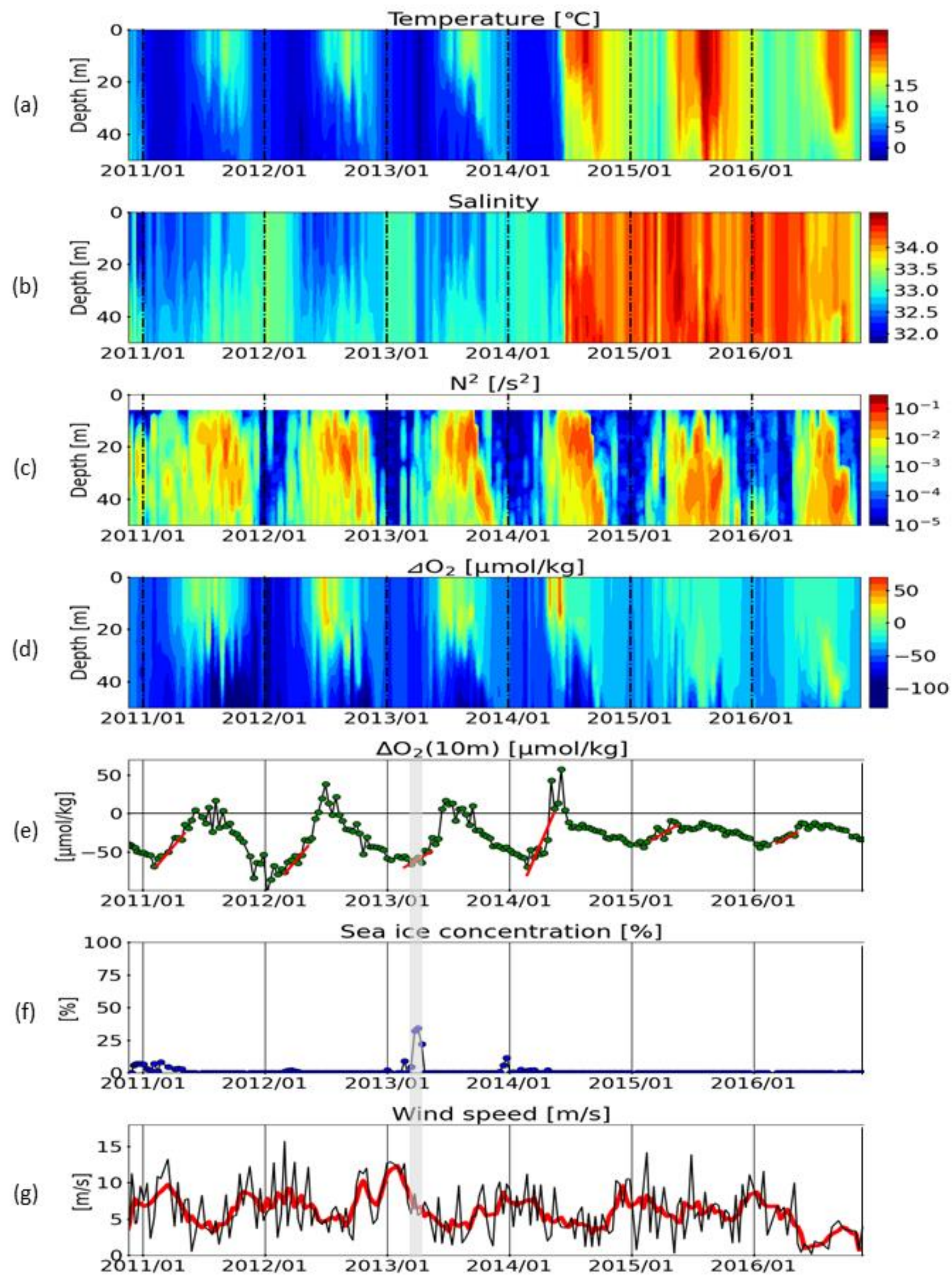

Figure S2

Time series of vertical profiles of (a) temperature, (b) salinity, (c) buoyancy frequency squared, represent as N^2, (d) ΔO_2 and (e) ΔO_2 at 10m for float 6404 (cyan in Fig.1) and (f) sea-ice concentration from SSM/I and (g) wind speed from ECMWF. The red lines in (e) indicate least-squares fitting, showing the increase rate of ΔO_2 during the spring bloom. The gray shades in (e)~(g) highlight the periods of sea-ice melt.

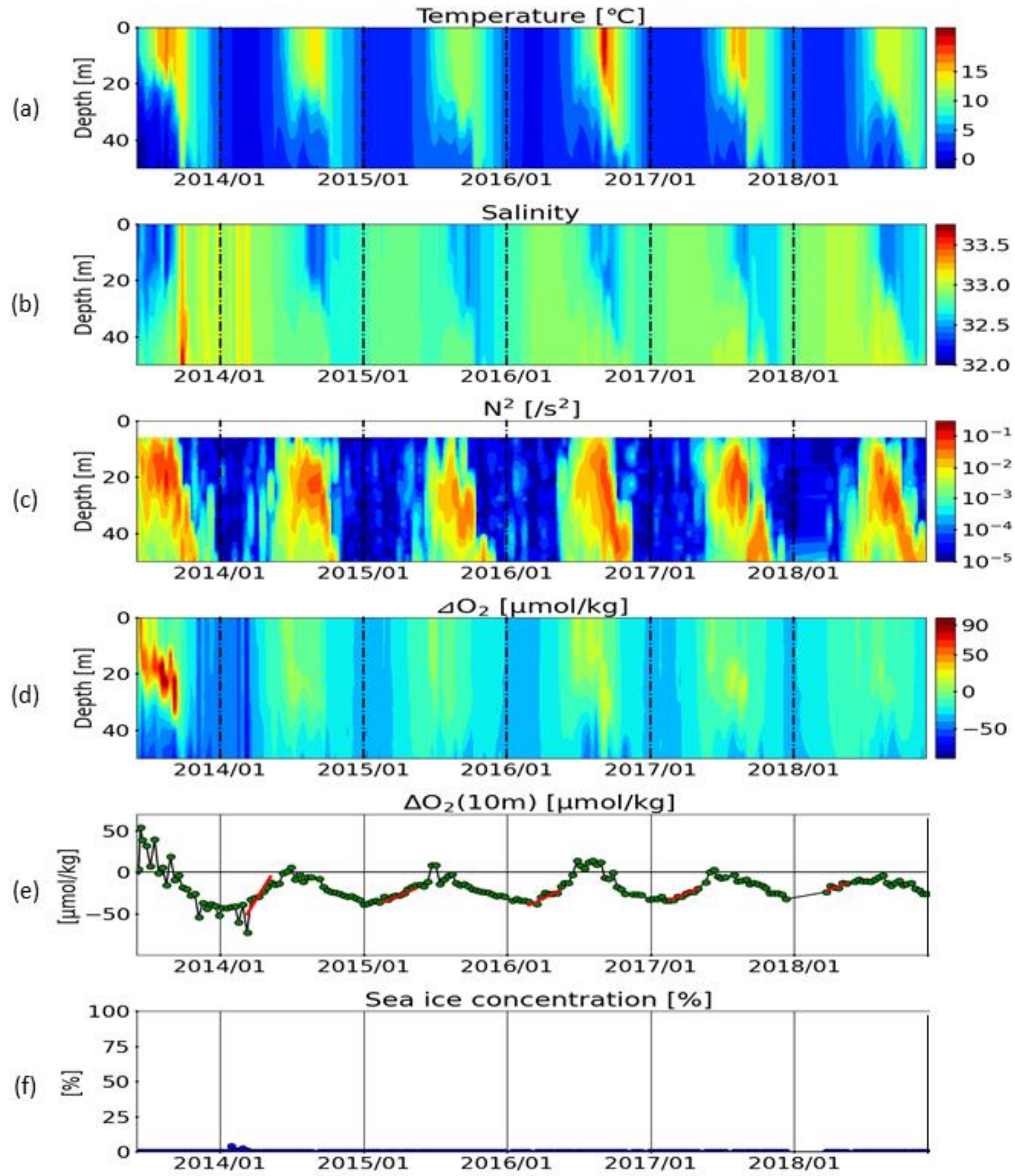

Figure S3

Time series of vertical profiles of (a) temperature, (b) salinity, (c) buoyancy frequency squared, represent as N^2, (d) ΔO_2 and (e) ΔO_2 at 10m for float 9001 (yellow in Fig.1) and (f) sea-ice concentration from SSM/I and (g) wind speed from ECMWF. The red lines in (e) indicate least-squares fitting, showing the increase rate of ΔO_2 during the spring bloom. The gray shades in (e)~(g) highlight the periods of sea-ice melt.

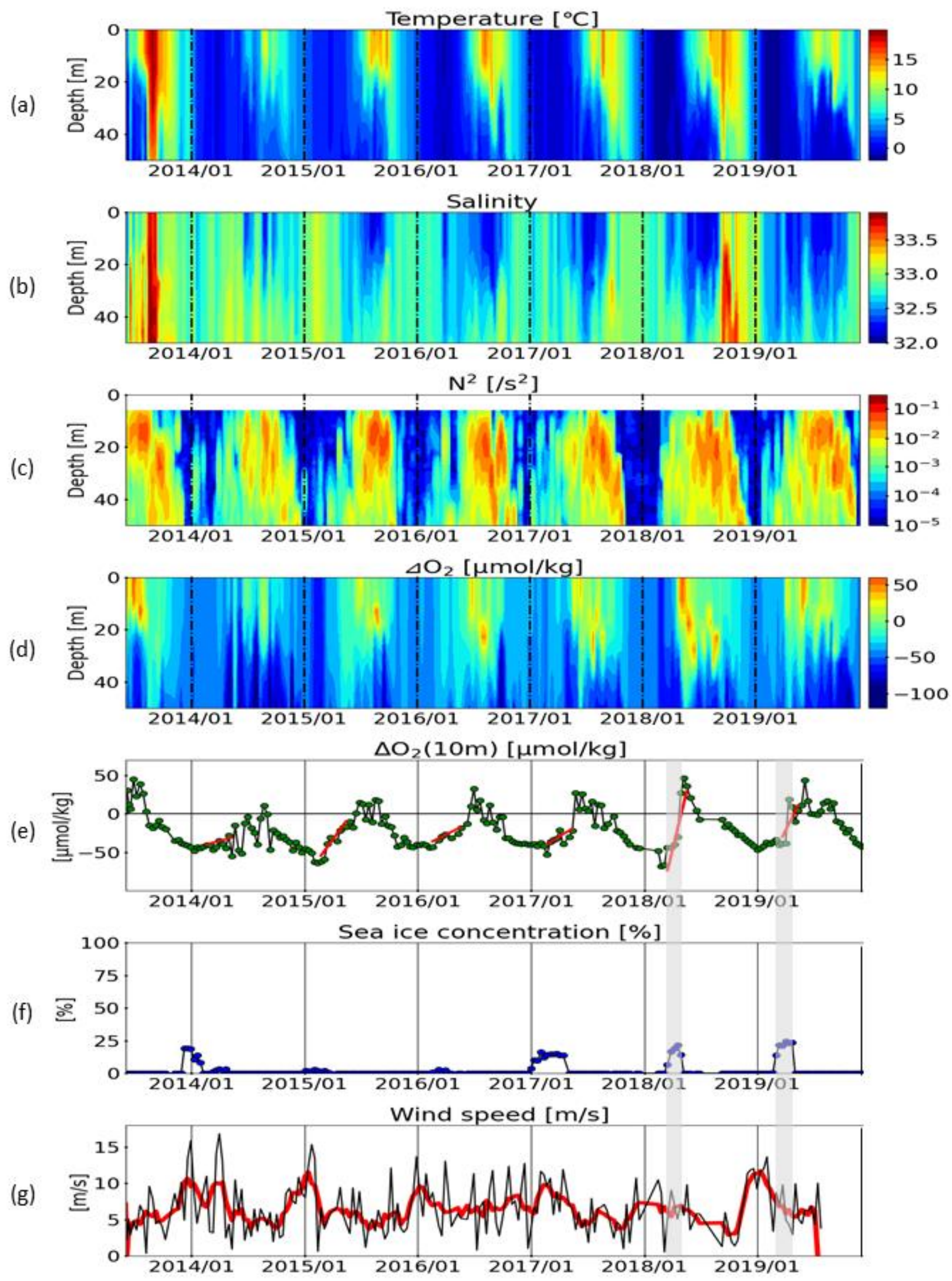

Figure S4

Time series of vertical profiles of (a) temperature, (b) salinity, (c) buoyancy frequency squared, represent as N^2, (d) ΔO_2 and (e) ΔO_2 at 10m for float 9021 (blue in Fig.1) and (f) sea-ice concentration from SSM/I and (g) wind speed from ECMWF. The red lines in (e) indicate least-squares fitting, showing the increase rate of ΔO_2 during the spring bloom. The gray shades in (e)~(g) highlight the periods of sea-ice melt.

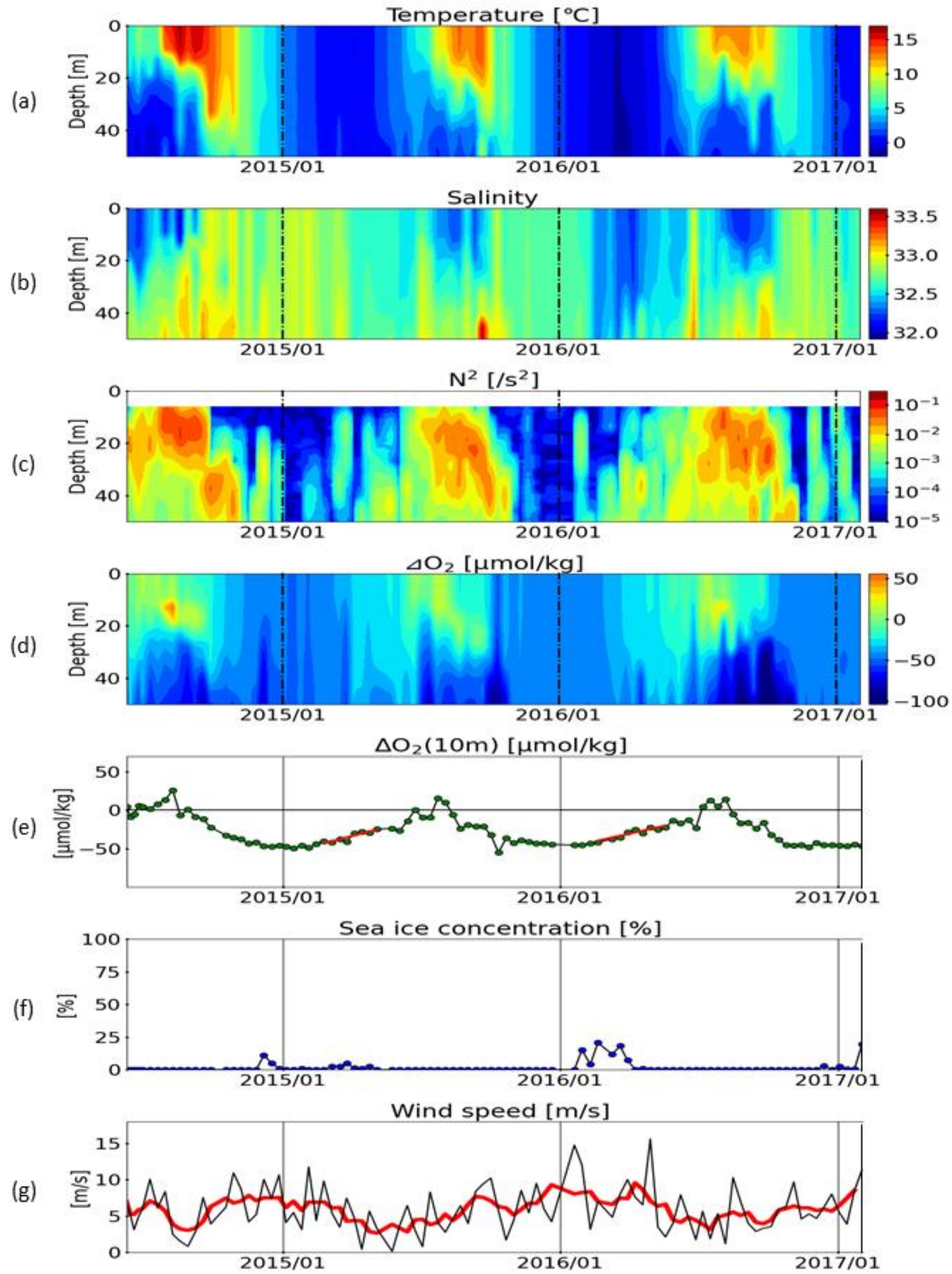

Figure S5

Time series of vertical profiles of (a) temperature, (b) salinity, (c) buoyancy frequency squared, represent as N^2, (d) ΔO_2 and (e) ΔO_2 at 10m for float 9049 (purple in Fig.1) and (f) sea-ice concentration from SSM/I and (g) wind speed from ECMWF. The red lines in (e) indicate least-squares fitting, showing the increase rate of ΔO_2 during the spring bloom. The gray shades in (e)~(g) highlight the periods of sea-ice melt.

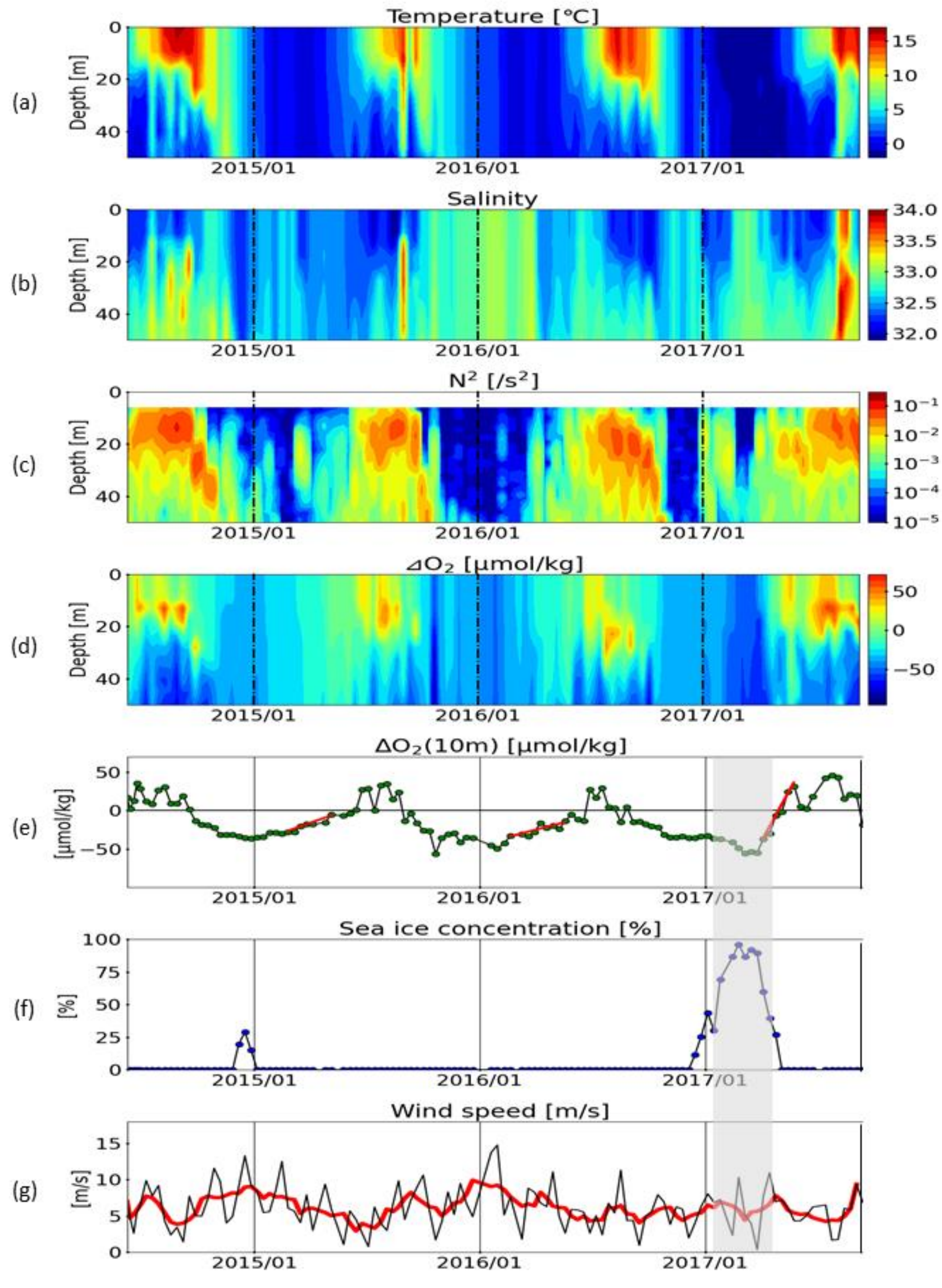

Figure S6

Time series of vertical profiles of (a) temperature, (b) salinity, (c) buoyancy frequency squared, represent as N^2, (d) ΔO_2 and (e) ΔO_2 at 10m for float 9050 (pink in Fig.1) and (f) sea-ice concentration from SSM/I and (g) wind speed from ECMWF. The red lines in (e) indicate least-squares fitting, showing the increase rate of ΔO_2 during the spring bloom. The gray shades in (e)~(g) highlight the periods of sea-ice melt.